Hypersonic Finite-Rate Chemically Reacting Viscous Flows over an Ablating Carbon Surface

D. J. Song*
Virginia Polytechnic Institute and State University, Blacksburg, Virginia
and
Clark H. Lewis†
VRA, Inc., Blacksburg, Virgina

Hypersonic finite-rate chemically reacting viscous flows over an ablating carbon surface have been analyzed using the viscous shock-layer method to study the effects of ablating carbon on the surface-measurable quantities and on the electron density, temperature, and species profiles across the shock layer. The results for nonequilibrium air injection and the ablating carbon surface mass transfer were compared. Of all the test cases considered, the ablating carbon case shows an approximately 10% higher stagnation heat-transfer rate than the equivalent nonequilibrium air injection case. The effects of fully catalytic, noncatalytic, and equilibrium catalytic wall boundary conditions were also compared to analyze the effects of catalytic wall boundary conditions on the heat-transfer rate. At low wall temperatures, such as 1000 K, the noncatalytic wall condition showed the lowest heat-transfer rate. However, at high wall temperatures (such as 3333 K) due to the positive wall diffusion heat transfer, the equilibrium catalytic wall condition showed the lowest heat-transfer rate at an altitude of 84 km and a freestream velocity of 7.6 km/s. A method for analyzing nonequilibrium finite-rate chemically reacting flows over multiconic geometries with ablating carbon surface has been developed.

Nomenclature

A_0-A_5 = coefficients of partial differential equations
B' = blowing parameter, $\dot{m}_T/C_H$
C_A = axial force coefficient
C_H = film coefficient, $q_c/(H_r - h_w)$
C_N = normal force coefficient
C_M = pitching moment coefficient
C_{FS} = skin-friction coefficient in the streamwise direction
C_i = concentration of species i, ρ_i/ρ
C_p = constant pressure specific heat
D_{ij} = diffusion coefficient
E-/CC = electron concentration per cubic centimeter
H = stagnation enthalpy, $H^*/U_\infty{}^2$
k = thermal conductivity
Le = Lewis number, $\rho C_p D_{ij}/k$
$\dot{m}$ = mass transfer rate, $\rho_w v_w/\rho_\infty U_\infty$
$\dot{m}_T$ = sum of char removal rate and pyrolysis gas rate
p = pressure, $p^*/\rho_\infty U_\infty^2$
q_c = convective heat-transfer flux
q_w = heat-transfer rate at the wall
R = gas constant
Re = Reynolds number
Rn^* = nose radius, m
S/RN = nondimensionalized streamwise distance
s,n,ϕ = nondimensional surface-normal coordinate system
T = temperature, T^*/T_{ref}
T_{ref} = $U_\infty^2/C_{p\infty}$
U_∞ = freestream velocity, m/s
u,v,w = velocity components in normalized surface-normal coordinates
x, X = axial length
Y = distance normal to body
Z_{CP}/L = location of center of pressure
α = angle of attack, deg
ϵ = Reynolds number parameter
ϵ^2 = $\mu_{ref}/\rho_\infty U_\infty Rn^*$
μ = viscosity, μ^*/μ_{ref}
ξ,η,ζ = normalized surface-normal coordinates
ρ = density, ρ^*/ρ_{ref}

Superscripts

( )* = dimensional variable

Subscripts

i = species i
ref = dimensional reference conditions
w = wall conditions
∞ = dimensional freestream conditions

Presented as Paper 84-1731 at the AIAA 19th Thermophysics Conference, Snowmass, CO, June 25-28, 1984; submitted July 13, 1984; revision received Jan. 10, 1985.

*Graduate Student, Aerospace and Ocean Engineering Department. Student Member AIAA.
†President. Associate Fellow AIAA.

Introduction

WHILE supersonic and hypersonic flows over blunt bodies have been of interest in fluid dynamics for many years, recent developments in aerodynamics and space flight have generated significant renewed interest in nonequilibrium viscous flowfield analyses of blunt multiconic re-entry vehicles. A major motivation for this has been the recent interest in the aeroassisted orbital transfer vehicles (AOTV), which use aerobreaking and aerocapture techniques at relatively high altitudes. At such altitudes, the characteristic reaction time is much longer than the characteristic flow time and the vehicle is in the chemical nonequilibrium flow regime for most of the time. Also, during aerocapture, the vehicle operates at reasonably high angles of attack. In addition to such AOTV applications, the presence of ionized species in the shock layer has a significant impact on the transmission of electromagnetic signals to and from the vehicle.

High-altitude hypersonic re-entry flows are, in general, characterized by low Reynolds numbers. Due to such typically low Reynolds number flows, the application of boundary-layer methods has encountered significant difficulties (such as displacement-thickness interaction, streamline tracking, deter-

mination of edge conditions, etc.) The nonequilibrium laminar boundary-layer analysis method of Blottner et al.[1] is a particular example of such solution methods. The viscous shock-layer (VSL) methods, on the other hand, have shown a great potential for analyzing such nonequilibrium viscous re-entry flows.

The perfect-gas VSL equations were originally derived from the full Navier-Stokes equations by Davis.[2] The VSL equations were subsequently modified by Davis[3] to include a chemically reacting binary gas mixture. Moss[4] further extended the VSL scheme to study a five-species (O, O_2, N, N_2, and NO) gas model. However, these studies were restricted to only analytic bodies such as hyperboloids. Miner and Lewis[5] extended the VSL scheme to study the axisymmetric flow around nonanalytic (sphere-cones) re-entry vehicles using the seven-species (O, O_2, N, N_2, NO, NO^+, and e^-) model of Blottner et al.[1] Swaminathan et al.[6] extended the axisymmetric VSL equations, for a seven-species reacting gas mixture, to study the three-dimensional nonequilibrium viscous flows around multiconic re-entry vehicles. They used a body-normal coordinate system and also coupled the solutions of the first-order continuity equation and the first-order normal momentum equation, resulting in increased stability of the VSL solution scheme. The subsequent work of Swaminathan et al.[7,8] involved an extension of their earlier work to study the effects of wall and/or shock-slip, fully catalytic wall conditions, noncatalytic wall conditions, and an 11 species gas model.

Kim et al.[9] extended the nonequilibrium VSL solution scheme to include a nonorthogonal coordinate system and studied the flowfield around the Space Shuttle orbiter. Their studies focused attention on the three-dimensional nature of the actual flowfield, as opposed to the "equivalent axisymmetric body method." Investigators have also studied and shown that (depending upon the flight altitude) finite-catalytic wall boundary conditions can significantly influence the wall heat transfer.[9] The nonequilibrium VSL solution schemes developed to date are applicable for conditions where the surrounding fluid consists of a reacting, dissociating, and ionizing mixture of air species. However, during hypersonic re-entry applications and for AOTV applications, the shock-layer temperature is very high and produces a significant amount of surface heating. This, in turn, can result in appreciable ablation of the surface material.

If the ablation products are in significant amounts, the gas chemistry in the shock layer can also be affected. Especially because of the different specific heats and heat of formations of the ablation products and their subsequent reactions with the surrounding gas species, the shock-layer temperature distribution can be quite different. Variations occur in the shock-layer heat transfer, the gas chemistry, the dissociation and ionization levels of the surrounding gases, electron concentration profiles, etc.

For many reasons carbon (graphite) is one of the most common thermal protection materials used, especially in the nose region of conventional re-entry vehicles. The two important ablation products from graphites, with moderate surface temperature at high altitudes and/or at conditions where ablation is due to chemical reaction between the carbon surfaces and the environmental gases (i.e., oxidative reactions) are carbon monoxide (CO) and carbon dioxide (CO_2). However, at lower altitudes, where heating is more severe, carbon ablation is due to sublimation and the prominent ablation products are the carbon vapor species C_1, C_2, C_3, C_4, C_5, etc. Scala and Gilbert[10] studied the hypersonic laminar stagnation heat transfer in gas mixtures with varying proportions of CO_2 and CO, using a boundary-layer approach. Their study shows that, depending upon the enthalpy content, these ablation products had an appreciable affect on the local temperature distribution. Although their study concentrated on the wake properties, the qualitative aspect of their results can also be applied to the shock-layer flow. Therefore, analyzing the effects of ablating carbon would be very helpful in understanding the phenomena during hypersonic flight conditions.

Analysis

In this paper, we have analyzed the nonequilibrium viscous flows around spherically blunted multiconic re-entry vehicles in a C-CO-CO_2-air mixture. A sphere-cone (9 deg)-cylinder-flare (5 deg) vehicle with nose radius 0.1524 m (refer to Fig. 1) at zero angle of attack and at 2 deg angle of attack is studied under hypersonic flight conditions. The freestream conditions correspond to a flight altitude of 84 km and velocity of 7.6 km/s.

The governing equations are derived from the steady Navier-Stokes equations for a reacting gas mixture (as given by Bird et al.[11]) and are written in surface-normal coordinates. The viscous shock-layer equations are parabolic in the cross-flow direction as well as in the streamwise direction. The detailed derivation of VSL equations for a chemically reacting air mixture was given by Swaminathan et al.[6]

Solution Procedure

The equations are written in standard parabolic form,

$$A_0\frac{\partial^2 W}{\partial\eta^2}+A_1\frac{\partial W}{\partial\eta}+A_2W+A_3+A_4\frac{\partial W}{\partial\xi}+A_5\frac{\partial W}{\partial\zeta}=0$$

The finite difference algorithm used to solve the ξ-momentum, ζ-momentum, energy, and species equations is the tridiagonal solver as used by Murray and Lewis.[12] The continuity and normal momentum equations are coupled together[13] to considerably enhance the overall numerical stability characteristics of the scheme.

The equations are solved in the following sequence: 1) eight species conservation (C_i), 2) ζ momentum (w), 3) energy (T), 4) ξ momentum (u), 5) integration of continuity for shock standoff distance (nsh), and 6) the coupled normal momentum (P) and continuity (v). The shock-layer equations depend on the shock slope ($\partial nsh/\partial\xi$) and normal velocity gradient along streamwise direction ($\partial v/\partial\xi$), which introduce an elliptic effect into the equations. In present code the shock slope ($\partial nsh/\partial\xi$) is provided externally by an inviscid code, NOL,[28] and the values of $\partial v/\partial\xi$ are calculated from a backward-difference formula.

Boundary Conditions

At the wall, the no-slip boundary conditions were used. The surface conditions are

$$u=w=0 \text{ and } T=T_w$$

where T_w is either a constant or a specified temperature variation. The species boundary conditions at the wall are discussed in the later section. The Rankine-Hugoniot jump conditions were used to obtain the properties behind the shock. The species concentration downstream of shock is frozen at the freestream species concentration.

The wall-slip, shock-slip, and temperature jump boundary conditions for rarefield gas were not considered in the present calculations.

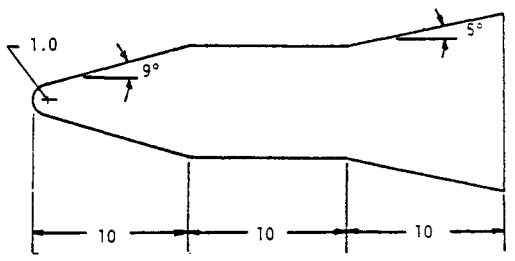

Fig. 1 Sphere-cone-cylinder-flare vehicle geometry.

Wall Temperature and Mass Injection Rate

Ablating mass transfer from the body surface occurs on most re-entry-type vehicles in passive heat shield protection applications. An energy balance at the surface can be used to obtain the surface mass transfer rates and wall temperatures by correlating theoretical and experimental results for the blowing parameter B' with the heat-transfer coefficient C_H. The quasiequilibrium $\dot{m}$ and T_w for a carbon surface have been calculated with the code developed by Thompson.[14] The empirical and theoretical basis for mass transfer models used in this study was presented by Hecht and Nestler,[15] who used a three-dimensional integral boundary-layer method for the steady-state calculation of ablation.

Figures 2 and 3 show the $\dot{m}$ and T_w distributions along the multiconic body, respectively. In the stagnation region, the procedure predicts approximately 4.5% mass transfer rate ($\rho_w v_w/\rho_\infty U_\infty$) and the wall temperature of 1778 K.

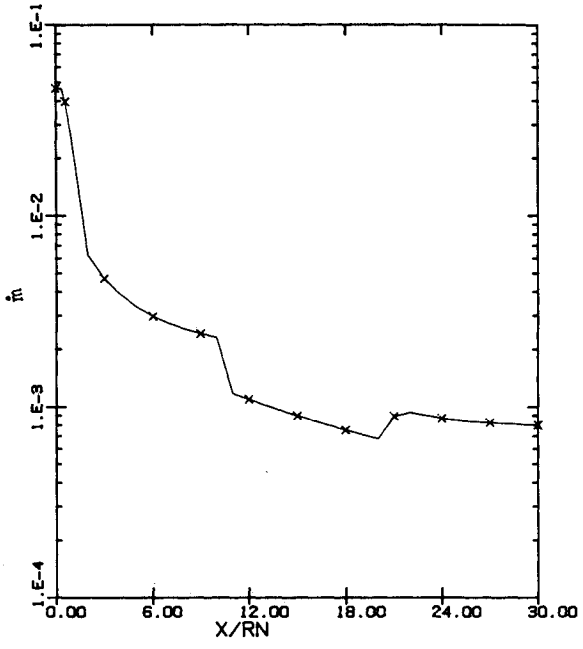

Fig. 2 Graphite ablation rate distribution along the body.

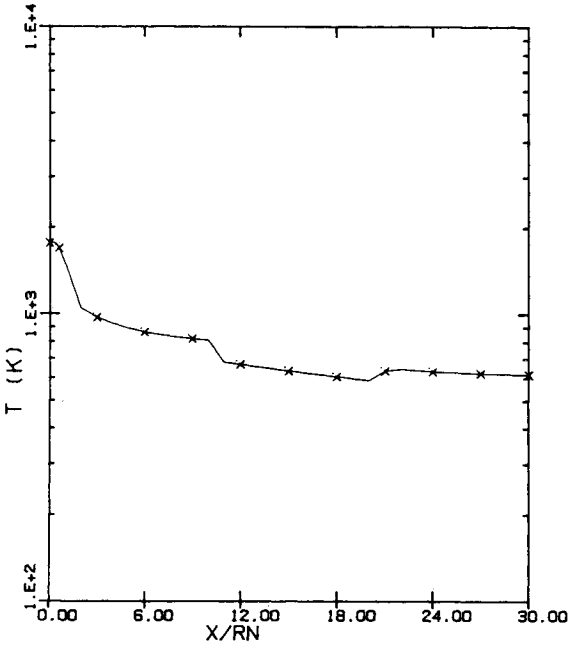

Fig. 3 Wall temperature distribution along the body.

Catalytic Surface Condition

We assumed that graphite (carbon) was burned at the wall, producing CO_2, CO_1, and carbon gas in equilibrium with air, even though the carbon-air mixtures are chemically reacting at a finite rate throughout the shock layer. Since we are dealing with gas-phase reactions at the wall, the effects of surface reactions (such as endothermic reactions) are not included in the present study. The "no mass transfer" fully catalytic wall boundary conditions for nonequilibrium air species can be written as,

$$C_{O_2} = 0.23456 \qquad C_{N_2} = 0.76544$$

$$C_O = C_{NO} = C_N = C_{NO+} = 0$$

The noncatalytic wall conditions are written as

$$\left(\frac{\partial C_i}{\partial \eta}\right)_w = 0$$

For the equilibrium catalytic wall,

$$C_i = C_{i-eq}(T_w)$$

In the present study C_{i-eq} has been obtained from the Gibbs free-energy ($G = H - TS$) minimization technique and provided as input data from the code developed by Gordon and McBride.[16] However, for the ablating carbon surface boundary conditions, only the equilibrium wall conditions have been used.

Thermodynamic and Transport Properties

The thermodynamic properties of the air mixture O, O_2, NO, NO^+, N_2, and CO are obtained from the thermodynamic data of Browne.[17-19] C and CO_2 data are obtained from Esch et al.[20] and Gordon and McBride[16] in the form of curve-fit relations. However, due to lack of thermodynamic properties of CO_2 at very high temperatures (above 10,000 K), we assumed a constant C_p above 10,000 K to calculate the enthalpy of CO_2. This is permitted because at high temperatures CO_2 is completely dissociated and has no contribution to either enthalpy or specific heat of the mixture. A second-order Lagrangian interpolation was used to obtain the values of H_i and C_{p-i} from the tables. The viscosity of each of the individual species was calculated from the curve-fit relation. The curve-fit constants for O, O_2, NO, N, NO^+, and N_2 are obtained from Blottner.[21] The coefficients for C, CO, and CO_2 are obtained from Moss.[22] The curve-fit constants are given in Table 1.

The thermal conductivity of the individual species was calculated from the Eucken semiempirical formula using the species viscosity and specific heat. After calculating the viscosities and thermal conductivities of individual species, the viscosity and thermal conductivity of the mixture was

Table 1 Viscosity curve fit coefficients of individual species[a]

Species	A_i	B_i	C_i
e-	0.0	0.0	0.0
N_2	0.048349	−0.022485	− 9.9827
O_2	0.038271	0.021076	− 9.5986
N	0.008586	0.6463	−12.581
O	0.020022	0.43094	−11.246
NO	0.042501	−0.018874	− 9.6197
NO+	0.042501	−0.018874	− 9.6197
C	0.092519	−0.908595	− 5.62783
CO	0.119888	−1.153705	− 5.22652
CO_2	0.119888	−1.153705	− 5.22652

[a] $\mu_i = \exp(C_i)\, T_k^{(A_i \ln T_k + B_i)}$, g/cm·s. Viscosity of CO_2 was assumed same as CO.

calculated using Wilke's semiempirical relations. The detailed formulas can be found from Swaminathan et al.[7] The diffusion model used in the present study is a limited binary diffusion model with binary diffusion coefficients specified by the Lewis number

$$Le = \rho C_p D_{ij}/k = 1.4$$

Chemical Reaction Model

It is assumed that the chemical reactions proceed at a finite rate and the rate of production $\dot{w}_i$ of the individual species are needed. For the present study, 10 species (O, O_2, NO, N, NO^+, N_2, C, CO, CO_2, and e^-) and 10 reaction rate equations were chosen to represent the flowfield over ablating carbon surfaces. They are

$$O_2 + M_1 = 2O + M_1 \quad (1)$$

$$N_2 + M_2 = 2N + M_2 \quad (2)$$

$$N_2 + N = 2N + N \quad (3)$$

$$NO + M_3 = N + O + M_3 \quad (4)$$

$$NO + O = O_2 + N \quad (5)$$

$$N_2 + O = NO + N \quad (6)$$

$$N + O = NO^+ + e^- \quad (7)$$

$$CO + O + M_4 = CO_2 + M_4 \quad (8)$$

$$CO + M_5 = C + O + M_5 \quad (9)$$

$$CO + O = C + O + O \quad (10)$$

Reactions 1-7 correspond to the seven-species model used by Blottner et al.[1] and Miner and Lewis[5] and are based on the data proposed by Bortner.[23] The reaction rate data for reaction 8 is based on the values recommended by Langan et al.[24]

Davies[25] determined that the dissociation of CO_2 can be approximated through multistep reactions. However, because of the difficulties in numerical implementation, the CO_2 dissociating mechanisms are limited to a single-step reaction as recommended by Langan et al.[24]

The reaction rate data for reactions 9 and 10 are based upon the recommendations of Appleton,[26] although the backward reaction rate constants for reactions 9 and 10 are obtained from the equilibrium constants given by Schofield.[27] The reaction rate data are tabulated in Table 2.

Results and Discussion

In this reaction, the predictions of the new VSL nonequilibrium code for carbon- air mixture (with equilibrium catalytic wall conditions) are compared with the nonequilibrium air-injection results (VSL7S) with fully catalytic wall conditions. A no-mass-injection case is also presented to compare the effects of an ablating carbon surface on the nonequilibrium flowfield around a typical re-entry vehicle.

Effects of Ablating Carbon Surface on the Species Profile

The species concentration profile in the stagnation region for the test case is shown in Fig. 4. Figure 4 shows a monotonic increase in the O_2 and N_2 concentration profiles as one moves away from the equilibrium wall, while CO_2 dissociates quickly to produce O and CO, and due to the chemically frozen shock crossing condition, recombine near the shock.

Shock-Layer Temperature

The shock-layer temperature profiles predicted by both the present code and the VSL7S code are shown in Fig. 5. In Fig. 5, the maximum temperature difference between carbon injection and nonequilibrium air injection for the test case considered is approximately 610 K. The different heat capacities and heats of formation can be responsible for altering the gas temperature and species concentrations.

Electron Number Density

The electron number density profiles in the stagnation region and at $S/RN = 1.5$ are shown in Fig. 6. When compared with the seven-species air model (VSL7S), the present code (VSLNQC) predicts a slightly lower electron number density; however, the difference between the two codes is negligible.

Table 2a Reaction rate data for 10 species model,[a] cm^3/moles·s

Reaction	C_{0r}	exp (C_{0r})	C_{1r}	C_{2r}	D_{0r}	exp (D_{0r})	D_{1r}	D_{2r}
1	42.7302	3.61E+18	59400	−1	35.6407	3.01E+15	0	−0.5
2	39.7963	1.92E+17	113100	−0.5	36.9275	1.09E+16	0	−0.5
3	52.0800	4.15E+22	113100	−1.5	49.1959	2.32E+21	0	−1.5
4	47.4305	3.97E+20	75600	−1.5	46.0617	1.01E+20	0	−1.5
5	21.8801	3.18E+09	19700	1.0	27.5933	9.63E+11	3600	0.5
6	31.8431	6.75E+13	37500	0.0	30.3391	1.50E+13	0	0.0
7	22.9238	9.03E+09	32400	0.5	44.3369	1.80E+19	0	−1.0
8	36.8414	1.00E+16	1761	0.0	46.1379	1.09E+20	65032	−0.58
9	62.6922	1.69E+27	129000	−2.86	54.8070	6.34E+23	−2116	−2.42
10	35.9571	4.13E+15	98025	0.0	28.0719	1.55E+12	−33091	0.44

[a]Reaction rate constants:
$K_{fr} = T_k^{C_{2r}} \exp(C_{0r} - C_{1r}/T_k)$, $K_{br} = T_k^{D_{2r}} \exp(D_{0r} - D_{1r}/T_k)$
T_k is in degrees Kelvin.

Table 2b Catalytic third-body efficiencies relative to argon $Z_{(j-ns),i}$

		O	O_2	NO	N	NO+	C	CO	CO_2	N_2
		$i=1$	2	3	4	5	6	7	8	9
$(j-ns)=1$	M1	25	9	1	1	0	0	0	0	2
2	M2	1	1	1	0	0	0	0	0	2.5
3	M3	20	1	20	20	0	0	0	0	1
4	M4	2	2	2	2	0	0	2	5	2
5	M5	0	0	0	0	0	0	2	0	0
6	e−	0	0	0	0	1	0	0	0	0

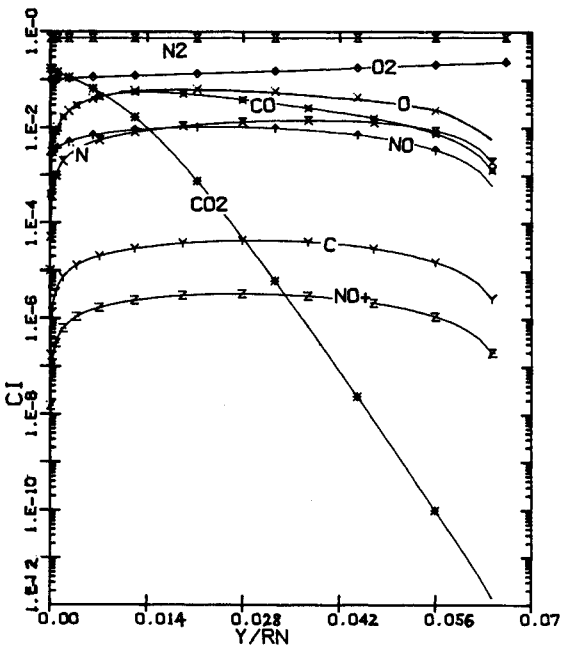

Fig. 4 Species concentration profile at stagnation point.

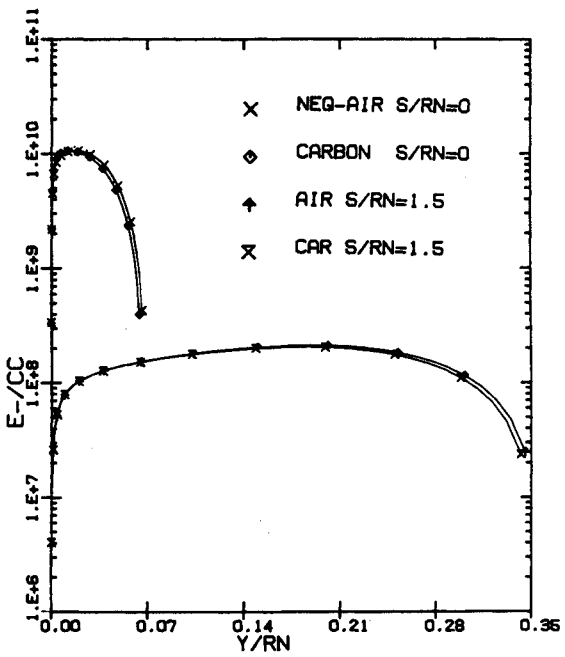

Fig. 6 Electron density profile at $s/Rn = 0$, and 1.5 at $\alpha = 0$ deg.

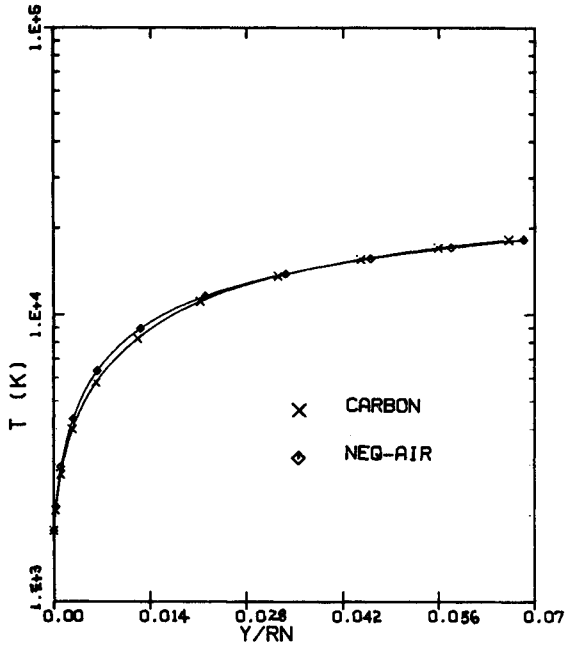

Fig. 5 Temperature profile through shock-layer at stagnation point ($\alpha = 0$ deg).

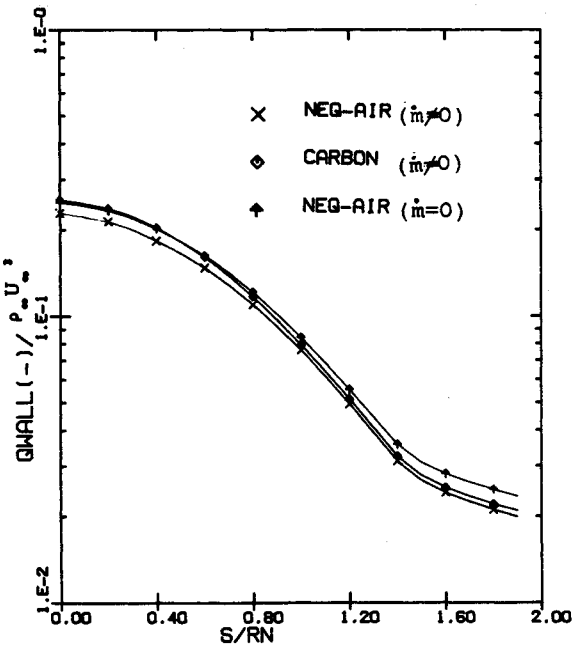

Fig. 7 Heat-transfer distribution over nose region ($\alpha = 0$ deg).

This is understandable because in both codes the only electron-producing equation is reaction 7. Also, carbon injection does not influence the electron number density significantly.

Surface-Measurable Quantities at Zero Angle of Attack

The effects of carbon injection through ablation in the nose region are shown in Fig. 7, whereas Fig. 8 shows these effects in the afterbody region. The case with carbon injection is compared with those having nonequilibrium air injection and the no mass injection. The results indicate that the wall pressures do not differ significantly.

Figure 7 shows some interesting differences in the heat-transfer rate between the carbon injection and nonequilibrium air injection cases. The nonequilibrium air injection case shows 11% lower values of the heat-transfer rate in the stagnation region. The carbon injection case was observed to have a slightly lower heat-transfer rate than the no injection case in the stagnation region. However, Fig. 8 shows that, in the afterbody region, the case with mass injection has a substantially lower heat-transfer rate than that with none.

Effects of Angle of Attack

The effects of angle of attack on the surface heat-transfer rate along the full-body for the high-altitude case are presented in Fig. 9. As shown in Fig. 9, there was no detectable difference in heat-transfer distribution between the two codes.

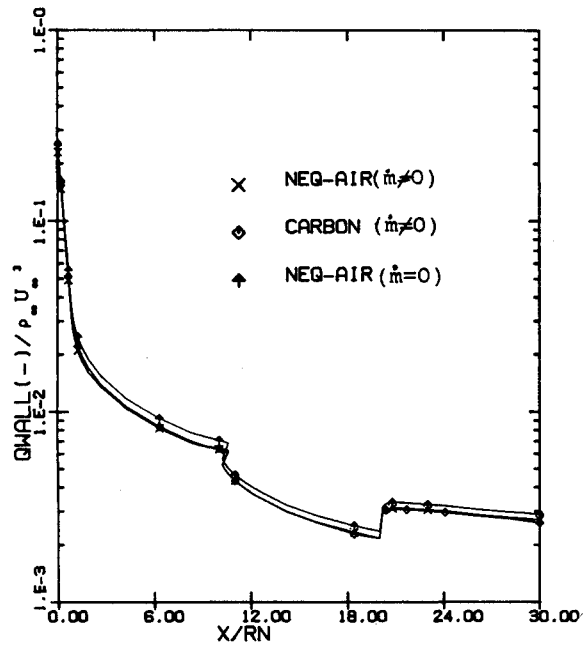

Fig. 8 Heat-transfer distribution along the body ($\alpha = 0$ deg).

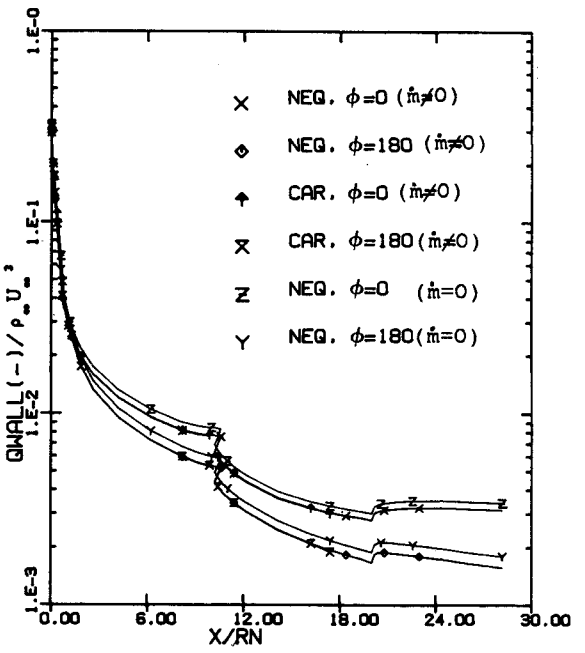

Fig. 9 Heat-transfer distribution along the body ($\alpha = 2$ deg).

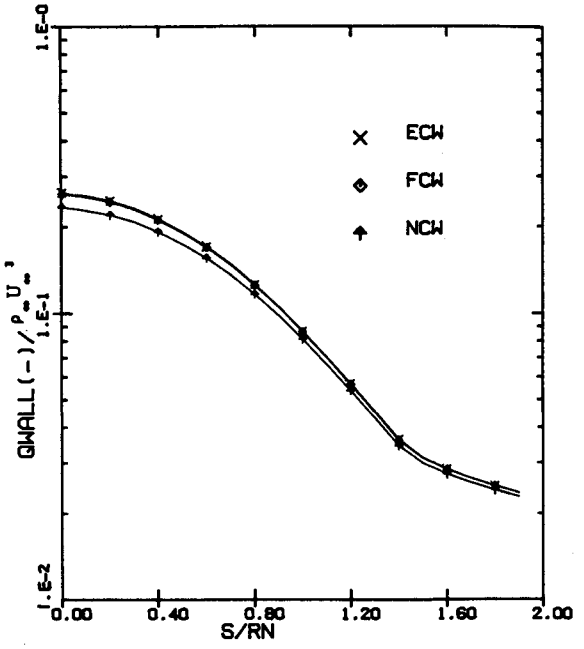

Fig. 10 Heat-transfer distribution over nose region for different boundary condition at 84 km, $\alpha = 0$, $T_{wall} = 1000$ K.

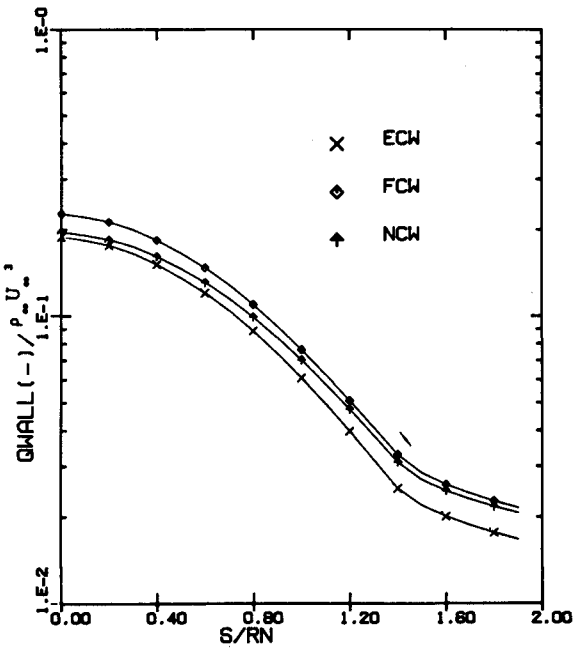

Fig. 11 Heat-transfer distribution over nose region for different boundary conditions at 84 km, $\alpha = 0$, $T_{wall} = 3333$ K.

Force and Moment Coefficients

Force and moment data obtained from various calculations are presented in Table 3. The differences between the present code and VSL7S with mass transfer were almost negligible. However, the differences in the axial force coefficient between the mass transfer and no mass transfer cases were about 6%.

Catalytic Wall Conditions

Figure 10 shows the effects of catalytic wall boundary conditions on the surface heat-transfer rate without mass transfer for a wall temperature of 1000 K. Differences of approximately 10% in the heat-transfer rate were observed in the stagnation region between the noncatalytic wall (NCW) and the fully catalytic wall (FCW) cases. The differences in heat-transfer rates in the stagnation region for the equilibrium catalytic wall (ECW) and the FCW cases were negligible. These results suggest that the surface temperature is low enough not to cause any significant dissociation or ionization of species. Since there is no diffusion heat transfer for the NCW condition, the NCW can be used as a lower limit in the prediction of heat-transfer rate for the cold-wall case.

The effects of the catalytic wall boundary conditions on the heat-transfer rate at a wall temperature of 3333 K with no mass injection are shown in Fig. 11. For these conditions, the ECW case shows the lowest prediction of heat-transfer rate, the NCW case is in the middle, and the FCW case is the highest. The negative gradient of species concentration (O and N_2) resulted in a positive diffusion heat-transfer at the stagnation point (as shown in Table 4). This means that for a hot

Table 3 Force and moment coefficients[a]

Case		$\alpha=0$ C_A	C_A	$\alpha=2$ C_N	C_M	Z_{CP}/L
NOL[b]PG	($\dot{m}=0$)	0.189008	0.185576	0.039164	−0.01534	0.391688
VSL7S	($\dot{m}=0$)	0.591844	0.615725	0.058187	−0.02734	0.469862
VSL7S	($\dot{m}\neq 0$)	0.554895	0.58083	0.055905	−0.026303	0.47049
VSLNQC	($\dot{m}\neq 0$)	0.557519	0.580297	0.056090	−0.026384	0.470385

[a]All data were obtained at the cylinder and flare juncture point. [b]Inviscid code developed by Solomon et al.[28]

Table 4 Stagnation heat-transfer rate,[a] MW/m²

Case	Conduction	Diffusion	Total
ECW	−0.89236	0.06582	−0.82654
FCW	−0.86457	−0.13133	−0.99590
NCW	−0.86201	0.00002	−0.86199

[a]Altitude 83.8 km, velocity 7.62 km/s case, and wall temperature of 3333 K.

Table 5 Computing time[a]

α, deg	$U\infty$, (m/s)	Method	ξ	Grid size of ξ steps	η points	ζ planes	Time (min:s)	ratio[b]
0	7620	VSL7S	0.0-30.8	61	51	1	2:24	1.00
2	7620	VSL7S	0.0-30.8	61	51	9	21:41	8.97
0	7620	VSLNQC	0.0-30.8	61	51	1	4:07	1.70
2	7620	VSLNQC	0.0-20.6	46	51	9	27:05	

[a]CPU time on IBM 370/3081, H = OPT2 compiler. [b]VSL7S for 84 km has been chosen as a reference value to calculate time ratio.

wall the equilibrium catalytic wall could be used as a lower limit to predict the heat transfer in the nose region.

Computing Times

The computing time required for each test case on the IBM 370/3081 (with H-compiler and OPT = 2 optimization) is shown in Table 5.

Conclusions

A code for analyzing three-dimensional hypersonic finite-rate chemically reacting flows over multiconic bodies with ablating carbon surfaces has been developed. The surface pressure distributions show no difference between the carbon injection and equivalent nonequilibrium air injection cases. However, the carbon injection code predicted approximately 10% higher heat-transfer rates in the stagnation region than the corresponding nonequilibrium air injection code. A shock-layer temperature drop of approximately 610 K was observed in the nose region for the high-altitude case. The electron number density differences observed were almost negligible. The equilibrium catalytic wall effects on the surface-measurable quantities were almost the same as those with the fully catalytic wall for the cold-wall case. However, in the case of a hot wall, the equilibrium catalytic wall predicted the lowest heat transfer. The aerodynamic force and moment coefficients at the cylinder/flare juncture were also computed. The differences in axial force coefficients between the present code and the seven-species nonequilibrium code (VSL7S) were negligible. In conclusion, a method for analyzing non-equilibrium finite-rate chemically reacting flows over multiconic geometries with ablating carbon surfaces has been developed. This method could be further extended to consider other ablating materials such as teflon and epoxy.

References

[1]Blottner, F. G., Johnson, M., and Ellis, M., "Chemically Reacting Viscous Flow Program for Multi-Component Gas Mixtures," Sandia Laboratories, Albuquerque, NM, Rept. SC-RR-70-754, Dec. 1971.

[2]Davis, R. T., "Numerical Solution of Hypersonic Viscous Shock-Layer Equations," *AIAA Journal*, Vol. 8, May 1970, pp. 843-851.

[3]Davis, R. T., "Hypersonic Flow of a Chemically Reacting Binary Mixture Past a Blunt Body," AIAA Paper 70-805, July 1970.

[4]Moss, J. N., "Solutions for Reacting and Nonreacting Viscous Shock Layers with Multicomponent Diffusion and Mass Injection," PhD Dissertation, Virginia Polytechnic Institute and State University, Blacksburg, Oct. 1971.

[5]Miner, E. W. and Lewis, C. H., "Hypersonic Ionizing Air Viscous Shock-Layer Flows over Nonanalytic Blunt Bodies," NASA CR-2550, May 1975.

[6]Swaminathan, S., Kim, M. D., and Lewis, C. H., "Non-equilibrium Viscous Shock-Layer Flows over Blunt Sphere-Cones at Angles-of-Attack," *Journal of Spacecraft and Rockets*, Vol. 20, July-Aug. 1983, pp. 331-338.

[7]Swaminathan, S., Kim, M. D., and Lewis, C. H., "Three-Dimensional Viscous Shock-Layer Flows over Complex Geometries," *AIAA Journal*, Vol. 22, June 1984, pp. 754-755.

[8]Swaminathan, S. and Lewis, C. H., "Effects of Chemical Modelling on Three-Dimensional Nonequilibrium Viscous Shock-Layer Flows," AIAA Paper 83-1425, June 1983.

[9]Kim, M. D. and Lewis, C. H., "Three-Dimensional Non-equilibrium Viscous Flow over the Shuttle with Surface Catalytic Effects," AIAA Paper 83-1426, June 1983.

[10]Scala, S. M. and Gilbert, L. M., "Theory of Hypersonic Laminar Stagnation Region Heat Transfer in Dissociating Gases," General Electric, Valley Forge, PA, Rept. TIS R63SD40, April 1963.

[11]Bird, R. B., Stewart, W. E., and Lightfoot, E. N., *Transport Phenomena*, John Wiley & Sons, New York, 1960.

[12]Murray, A. L. and Lewis, C. H., "Hypersonic Three-Dimensional Viscous Shock-Layer Flow over Blunt Bodies," *AIAA Journal*, Vol. 16, Dec. 1978, pp. 64-69.

[13]Murray, A. L. and Lewis, C. H., "Three Dimensional Fully Viscous Shock-Layer Flows over Sphere-Cones at High Altitudes and High Angles of Attack," Virginia Polytechnic Institute and State University, Blacksburg, Rept. VPI-AERO-078, March 1975.

[14]Thompson, R. A., "Viscous Shock Layer Flows over Multiconic Reentry Vehicles," MS Thesis, Virginia Polytechnic Institute and State University, Blacksburg, May 1983.

[15]Hecht, A. M. and Nestler, D. E., "A Three Dimensional Boundary-Layer Computer Program for Sphere-Cone Type Reentry Vehicles, Vol. I: Engineering Analysis and Code Description," AFFDL-TR-78-67, June 1978.

[16]Gordon., S. and McBride, B. J., "Computer Program for Calculation of Complex Chemical Equilibrium Compositions, Rocket Performance, Incident, and Reflected Shocks, and Chapman-Jouguet Detonations," NASA SP-273, March 1976.

[17]Browne, W. G., "Thermodynamic Properties of Some Atoms and Atomic Ions," General Electric Co., Philadelphia, MSD Engineering Physics, Rept. TM2, 1962.

[18]Browne, W. G., "Thermodynamic Properties of Some Diatomic and Linear Polyatomic Molecules," General Electric Co., Philadelphia, MSD Engineering Physics, Rept. TM3, 1962.

[19]Browne, W. G., "Thermodynamic Properties of Some Diatomic and Diatomic Ions at High Temperatures," General Electrical Co., Philadelphia, MSD Advanced Aerospace Physics, Rept. TM8, May 1962.

[20]Esch, D. D., Siripong, A., and Pike, R. W., "A Technical Report on Thermodynamic Properties in Polynomial Form for Carbon, Hydrogen, Nitrogen, and Oxygen Systems from 300 to 15000 K," NASA-RFL-TR-70-3, Nov. 1970.
[21]Blottner, F. G., "Nonequilibrium Laminar Boundary Layer Flow of Ionized Air," General Electric Co., Philadelphia, Rept. R64SD56, Nov. 1964.
[22]Moss, J. N., Private communication, April 1984.
[23]Bortner, M. H., "Chemical Kinetics in a Re-entry Flow Field," General Electric Co., Valley Forge, PA, Rept. TIS R63SD63, Aug. 1963.
[24]Langan, W. T., Cresswell, J. D., and Browne, W. G., "Effects of Ablation Products on Ionization in Hypersonic Wakes," General Electric Co., Valley Forge, PA, Rept. TIS 65SD208, Jan. 1965.
[25]Davies, W. O., "Carbon Dioxide Dissociation at 6000 K to 11000 K," *Journal of Chemical Physics*, Vol. 43, Oct. 1965, pp. 2809-2818.
[26]Appleton, J. P., Steinberg, M., and Liquornik, D. J., "Shock-Tube Study of Carbon Monoxide Dissociation Using Vacuum-Ultraviolet Absorption," *Journal of Chemical Physics*, Vol. 52, No. 5, 1970, pp. 2205-2221.
[27]Schofield, K., "Evaluated Chemical Kinetic Rate Constants for Various Gas Phase Reactions," *Journal of Physical and Chemical Reference Data,* Vol. 2, No. 1, 1973, pp. 25-84.
[28]Solomon, J. M., Ciment, M., Furguson, R. E., Bell, J. B., and Wardlow, A. B. Jr., "A Program for Computing Steady Inviscid Three-dimensional Supersonic Flow on Reentry Vehicles, Vol. 1: Analysis and Programming," Naval Surface Weapon Center, White Oak, MD, Rept. NSWC/WOL/TR 77-28, Feb. 1977.